Detailed Laser based investigations of the dynamic of spray combustion inside a multipoint injection system

L. Zimmer*, T. Providakis, P. Scouflaire, S. Ducruix

CNRS, UPR 288 "Laboratoire d'Energetique moleculaire et macroscopique, combustion"
Grande Voie des Vignes, 92295 Chatenay-Malabry
Ecole Centrale Paris, Grande Voie des Vignes, 92295 Chatenay-Malabry

laurent.zimmer@ecp.fr, theodore.providakis@ecp.fr, philippe.scouflaire@ecp.fr and sebastien.ducruix@ecp.fr

Abstract

In order to reduce pollutant emissions from aircraft engines, new strategies are used to to introduce the fuel in the combustion chamber. Those strategies tend to enhance mixing and reduce combustion temperature using partially premixed flames. However, this may lead to combustion instabilities, such as blow-off or strong coupling with pressure oscillations. To study the strategies of injecting fuels through different stages, a laboratory scaled combustor has been developed and runs at atmospheric pressure with dodecane as fuel. The fuel is injected through two, co-swirling stages. The first, using full cone, pressurized nozzle with 20% of air massflow rate is called the pilot stage. The second stage consists of a swirler in which 80% of the air flows and fuel is injected through 10 equally spaced holes of 0.3 mm diameter. The second stage is called the take-off stage. Air is preheated at 473K and a typical air massflow rate of 50 g/s is used for the experiments. A staging parameter α is defined as being the ratio of the mass of fuel injected through the pilot stage to the overall mass of fuel. In this paper, only one value of the staging parameter (α =60%) is deeply analyzed, even tough a different values of α (20%) is used to illustrate the different behavior observed. Different laser diagnostics are applied in both non-reacting and reacting conditions to understand the way the spray and the flame interact. A time resolved PIV measurement system is used to retrieve time resolved planar droplet velocities at 10 kHz. Furthermore, flame front position through OH-PLIF, at a lower frequency is used. Analysis of the results show appearance of a strong aerodynamic structure around frequencies of the order of 2500 Hz that is linked to the precessing vortex core (PVC). This structure still exists in reacting conditions and in some cases is strengthened when the flame is stabilized by the pilot. Reacting cases show also a peak at lower frequency (300Hz) associated to quarter wavelength of the combustion chamber. Two different flame structures are found : pilot or rim stabilized. This leads to the existence of a hysteresis phenomena with two different flame structure possible, despite having identical injection condition. Detailed analysis shows that for the rim stabilized flame, the main reaction front lies in the inner part of the chamber whereas the spray is in the outer part. For the flame stabilized by the inner recirculation zone, the main reaction front lies in the outer part of the spray in droplets stay in the inner side. This leads to different delays for evaporation and therefore different coupling with the acoustic mode of the combustion chamber. Furthermore, for one case, the PVC is strengthened, leading to a very stable flame whereas it is weakened in the second case, letting the flame be driven then by acoustic coupling.

Introduction

Reducing pollutant emission for aeronautical applications still remains a challenge. Lean premixed combustion systems offering lower temperatures are prone to intrinsic instabilities such as potential coupling between heat release and pressure fluctuations or to blowoff events. One possibility for better controlling the operations is to use a staging of the fuel. Part of the fuel may be introduced through a pilot injector, to stabilize the flame ([1]). The other part may be introduced more homogeneously inside the combustion chamber through a multiple hole approach. Many studies have been performed to show the dynamic behavior of gaseous burner using time resolved data (see [2] and subsequent works) or multiple planar imaging techniques [3]. Typical output power of those burners are of the order of 30 kW. Different analysis have been used to understand the complex dynamics in such gaseous burners, including phase-lock measurements or proper orthogonal decomposition approach. However, relatively limited informations are available for liquid-fueled burners. Among those, [4] proposed a detailed measurements of droplets based on phase Doppler anemometry and time series planar measurements to retrieve the diameter and the velocity of droplets as well as high-speed Mie scattering measurements. They operated their facility with

*Corresponding author: laurent.zimmer@ecp.fr

aviation kerosene Jet-A1 injected from a pressure atomizer and with preheated air. Typical Sauter mean diameter droplets were around 15 to 25 µm. They observed a different global behavior as identical operating conditions with a gaseous fuel. One of their main conclusion is that the spray is of importance in the appearance of self-excited combustion instabilities. A multi-point injection device was previously studied with gaseous fuel [1] and therefore, it is important to study the effects induced by a liquid fuel. The present article shows the typical self-excited instabilities in presence of liquid fuel. In the second section, the test rig developed is described. Third section is devoted to diagnostics and post-processing techniques. Fourth section will describe the dynamics of the combustion cases. Finally, conclusions as far as combustion stabilization will be presented in the last section.

Description of the experimental burner

The multipoint staged is composed of two stages where air and liquid fuel are mixed before entering a rectangular combustion chamber ($500 \times 150 \times 150$mm), composed of two silica windows for optical access and two water-cooled walls. The test bench is operated at atmospheric pressure. Dodecane is used as fuel in the present study. Its thermodynamical properties are relatively close to those of kerosene, while offering a good repeatability of experiments. A schematic view of the injection device is shown in Figure 1. Inside the injection device, the upstream (primary) stage is called the 'Pilot stage'. It is composed of a pressurized nozzle for fuel distribution and a swirler for air injection. The pressurized nozzle generates a solid cone and fuel can be injected at a maximum flow rate of 6.3 liters per hour. Its flow number is equal to $1.4\,\mathrm{l}\cdot\mathrm{h}^{-1}\cdot\mathrm{bar}^{-0.5}$. The air swirler is composed of 18 vanes and it is geometrically designed so that 20% of the global air rate flows through this stage. This has been checked experimentally in [1]. The downstream (secondary) stage is called the 'Takeoff stage'. It is composed of a multipoint system for the fuel and a swirler for the air. The multi-injection system is composed of 10 equally-spaced holes (0.3 mm in diameter). The swirler is composed of 20 vanes and it has been designed so that 80% of the global air rate flows through this stage. Both swirlers are set co-rotating and designed so that the swirl number S (ratio between the axial flux of the angular momentum and the axial thrust) based on geometrical considerations is close to 1 [5]. However, this swirl number decreases to reach about 0.40 as measured at the inlet of the combustion chamber. To enhance spray vaporization, only air is preheated at 473 K.

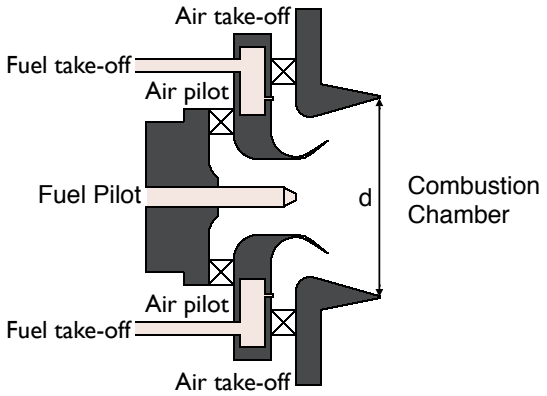

Figure 1. Schematic view of the injection device. Flow from left to right. Fuel main and air main are also designed as take-off stage.

As staging is one of the main features of this type of injection system, a staging factor α is defined to quantify the relative amount of fuel injected through the primary (pilot) injector [1]:

$$\alpha = \frac{\dot{m}_{f,p}}{\dot{m}_{f,g}} \times 100 \tag{1}$$

where $\dot{m}_{f,g}$ is the total fuel flow rate and $\dot{m}_{f,p}$ is the fuel flow rate through the primary stage. As a consequence, α will be zero in case all fuel flows through the secondary (take-off) stage and 100% for all fuel injected through the pilot stage.

Table 1. Operating and pressure conditions for both non-reactive and reactive conditions. $Pw = 85$ kW, $\phi = 0.6$, $P_a = P_{atm}$. Subscript t is for take-off while p is for pilot.

Condition	$\dot{m}_a$ [g · s^{-1}]	$\dot{Q}_{f,g}$ [l · h^{-1}]	$\alpha[\%]$
OP_{60}	53	9.4	**60**
Condition	$\Delta P_{f,t}$ [bar]	$\Delta P_{f,p}$ [bar]	$\Delta P_a/P_a$ [%]
OP_{60}	0.08	18	3 - 4

In the present paper, only one air mass flowrate will be presented (53 g.s^{-1}) for clarity. Table 1 shows the operating conditions chosen for the present study. The global air and fuel flow rates are kept constant (constant power and global equivalence ratio) while α is varied from 15 to 60%, a domain where the shape of the flame is highly influenced by the stage procedure. For values of α higher than 50% (pilot stage regimes), the flame stabilization process is controlled by the pilot stage, leading to a compact V-flame, anchored inside the injection device. For values of α lower than 25% (take-off stage regimes), the flame is stabilized thanks to the take-off stage and takes an M-shape. In-between, there seems to be a competition between both stages, leading to a tulip-like shape of the flame. In the present study, measurements focus on only one value of the staging factor (60%), as a strong double peak spectra has been obtained previously in the phase Doppler anemometer measurements [6]. This staging factor of 60 will be named OP_{60} in the following. The different pressure losses where measured in the pilot and take-off fuel as well as for the airflow. Results are reported in Table 1.

Experimental techniques and post-processing methods

To understand the mechanisms of flame stabilization, a time-resolved Particle Image Velocimetry technique is used. This diagnostic enables the determination of two components of the velocity of droplets at a sampling rate of 10 kHz. As it used in both non-reacting and reacting cases, a Scheimpflug configuration is used so as to get images in a plane perpendicular to the main flow. The schematic disposition of laser and camera is depicted in figure 2. The laser sheet is generated by a system consisting of two Nd:YAG lasers (*Quantronix*). Both lasers emit a pulse at a wavelength of 532 nm with an energy of 5 mJ and a temporal width of 120 ns. The laser is directed to the combustion chamber with a highly reflected mirror, able to sustain the overall laser power. An optical system (*Melles Griot*) is used to convert the laser beam into a planar light sheet 100 mm wide and 1 mm thick. Both sides of the combustion chamber contain rectangular silica windows allowing the laser sheet to cross horizontally the chamber, transverse to the main flow. A mechanical table (*Axmo*) is used to translate the laser sheet through the chamber, as well as the camera to keep images focussed.
A fast speed camera (Photron Fastcam, 576 × 576 pixels at a rate of 20000 frames per second) equipped with a 105 mm F/2.8 Nikon Nikkor objective is placed at two different positions towards the combustion chamber. The two lasers work at half of the camera's acquisition frequency and are synchronized by a pulse delay generator (BNC 555 pulse/delay Generator). When axial measurements are of interest, the laser sheet is introduced through a small window, placed at the bottom of the combustor and the camera is placed without a Scheimpflug adaptor.

The reaction zone is characterized using Planar Laser Induced Fluorescence (PLIF) measurements in axial planes. The PLIF technique is carried out by exciting the OH radical, which is a good tracer to describe the structure of the flame. The laser sheet is generated by a system consisting of a Nd:YAG laser (Continuum Powerlite DLS 8010 series), emitting a pulse at a wavelength of 532 nm, coupled to a Dye Laser (Continuum ND6000). The Dye laser possesses a UV Tracker that doubles the laser output. A cylindrical divergent and a spherical converging lenses with respective focal lengths at 250 mm and 300 mm are used to generate a laser sheet 70 mm wide and 1 mm thick. For this study, the excitation was at 282.904 nm. Images are acquired using an Intensified CCD camera (Princeton Instruments PI-MAP 3, 1024×1024 pixels at a rate of 15 images per second) equipped with a 105 mm F/4.5 Nikon Nikkor UV objective coupled to two interferential filters (Melles Griot, WG 305 and UG 11) centered on the OH radical emission band. Measurements are performed at 10 Hz and the exposure time of the camera was set to 100 ns. For each conditions and at each position, 1000 samples are taken.

In reacting conditions, pressure sensors as well as chemiluminescence sensors can provide the cyclic informa-

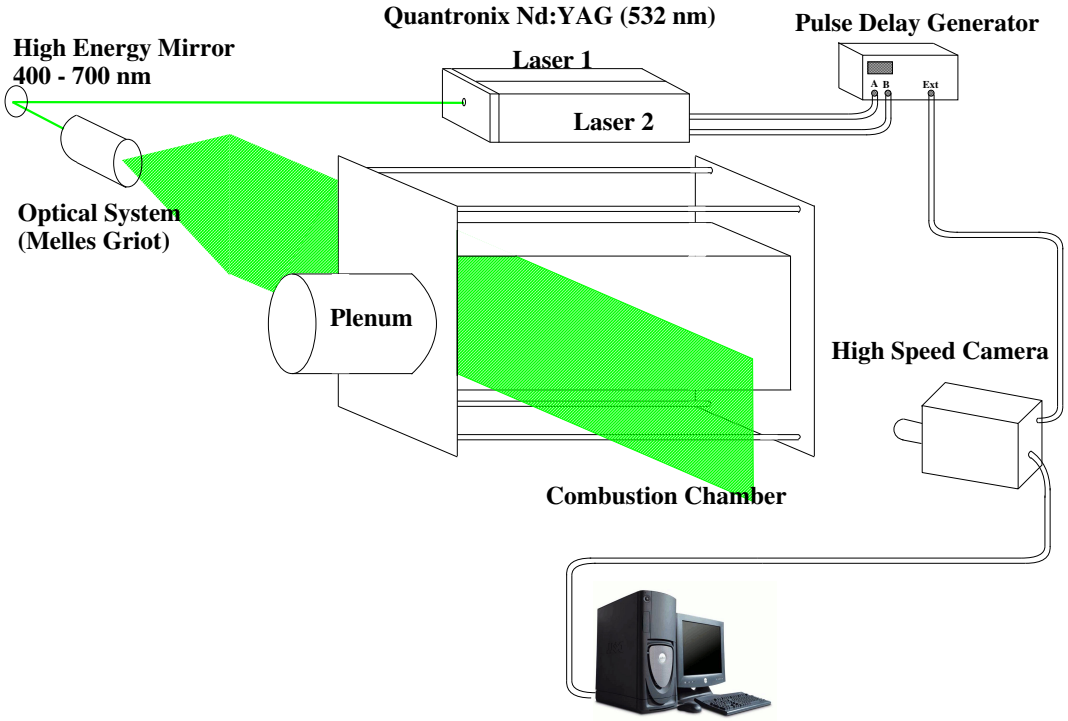

Figure 2. Schematic view of the time resolved Particle Image Velocimetry technique.

tion and enable reconstructing the full three-dimension modes. In the following, only the pressure signal from the pressure sensor located in the central axis of the combustion chamber and at 83 mm from the exit of the injection system. PIV algorithm is applied to the Mie scattering images. It is performed with an iterative procedure, starting with windows of 64 $\times$ 64 down to 16 $\times$ 16. At each step, a median filtering procedure is performed to remove outliers. No deformation of window is introduced through this process and the mean background is subtracted before making the PIV analysis. It is important to understand that the velocity field retrieved is close to a velocity weighted by the surface of each droplet [7].

Results and Discussion

Non reacting conditions

Detailed analyses of the non reacting conditions have been deeply addressed in a different paper ([6]) and here only the most important findings are summarized. Typical Sauter mean diameter was found to be encompassed between 15 to 25 µm, which represents a similar range as the one presented in [4]. It was also found that a strong peak arising around 2500Hz was strongly observed on Mie scattering images and velocity fields. The signal of the He-Ne laser was also showing this strong peak around 2500 Hz and it was possible to perform phase-lock measurements and to combine the dynamics of the different plane. This revealed that this frequency was clearly associated with a Precessing Vortex Core (PVC) movement. The center of the spray was seen to precess around the center of the injector ([8]).

Overall behavior for reacting cases

To ignite the mixture, all the fuel is first injected through the pilot stage and the overall flowrate of air is adjusted to 10 $g \cdot s^{-1}$. The air flowrate is then increased together with the pilot injection up to 30 $g \cdot s^{-1}$. At this value, mulitpoint injection system is also used to finally reach the overall air flowrate value of 50 $g \cdot s^{-1}$ with a high staging parameter : 60%. When looking at the flame obtained for this condition, name OP_{60} (see Figure 3), one can notice that the flame seems to be attached inside the pilot injection system. It is very compact as the main emission region is within 40 mm from the exit of the injection system. One can notice that the flame shape is of conical nature. When the staging parameter is decreased down to 20%, one can see that a complete different flame shape is obtained, as shown by the natural emission presented in Figure 4. This time, the flame seems to be lifted with a lift-off height of 70 mm. The flame seems to present a flat reaction zone. One has to recall that a staging

parameter of 20% means that 80 % of the fuel is injected through the multipoint system. This system tends to have homogeneous mixture all through the combustion chamber, hence leading to this kind of flame shape. This case is labelled OP_{20}. Most interestingly, when increasing again the staging parameter to 60%, one does not get the same flame shape as in the first case (see Figure 5). Whereas in the first case, the flame was anchored by the pilot, this second flame for 60%, named $OP_{60}H$, seems to be a double flame, showing both a strong emission close to the exit of the pilot as well as a flat reaction zone further downstream, at typically the same distance as for the OP_{20} case. Another difference compared to OP_{60} is that the angle of the reaction close to the pilot is much more straight. As the inlet conditions for OP_{60} and $OP_{60}H$ are exactly the same, one can conclude that there is some hysteresis phenomena and that only controlling the staging parameter does not guarantee to have a given flame shape.

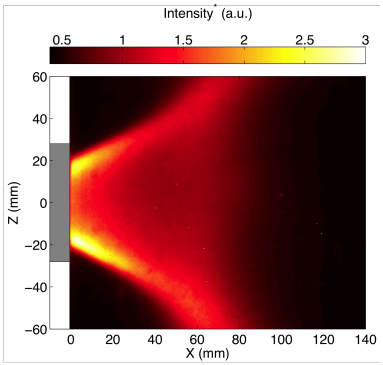

Figure 3. Natural emission of the flame for the pilot stabilized case for α=60% (OP_{60}).

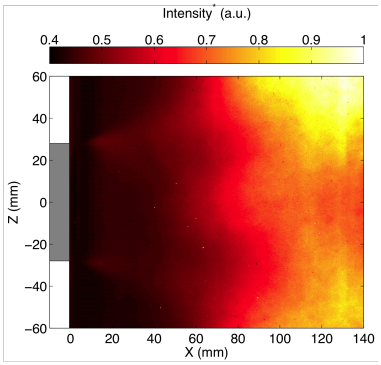

Figure 4. Natural emission of the flame for the chamber stabilized case for α=20% (OP_{20}).

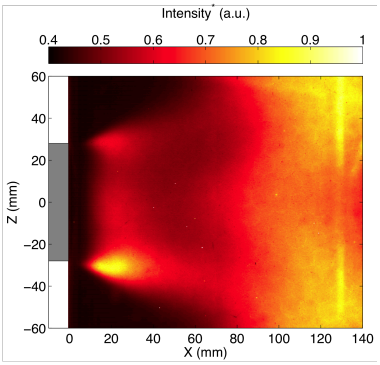

Figure 5. Natural emission of the flame for the chamber stabilized case for α=60% ($OP_{60}H$).

In parallel to natural emissions, it is possible to analyze the signals of the different pressure sensors. In reacting cases, those reveal several peaks, common to the different staging parameters (see Figures 6-8). The first peak is around 280 Hz to 300 Hz in the pressure field of both the plenum and the combustion chamber as well as the chemiluminescence signals. The second peak is around 2608 Hz and corresponds to the precessing vortex core (PVC). Its frequency has increased as compared to non-reacting cases, as expected by gaseous expansion. For the OP_{60} case, the peak associated to the PVC is very narrow whereas the low frequency is a bit broadener. This shows clearly that the PVC is very stable in frequency, helping stabilizing the flame. A the flame base has a precessing movement, its coherence with the quarter wavelength mode of the chamber is weakened, leading to an overall low pressure amplitude as well as a broad peak at low frequency. For the OP_{20} case, the situation is completely different. The peak associated to the PVC is very broad in frequency and has stronly diminished in amplitude. On the other side, the quarter wavelength mode has become narrow and multiple harmonics are found. The overall sound pressure level has increased from 138dB to 149dB. Finally, when increasing again the staging parameter and reaching $OP_{60}H$ case, one can notice that the pressure signatures remain identical as in OP_{20} case. This shows that the $OP_{60}H$ has a similar dynamic behavior as the OP_{20} case, even though having the same inlet conditions as OP_{60}. The overall sound pressure level has however decreased from 149dB for OP_{20} to 142 dB for $OP_{60}H$.

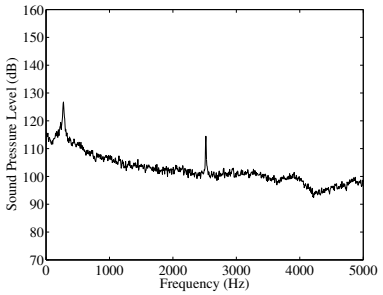

Figure 6. Pressure spectra in the combustion chamber for the OP_{60} case.

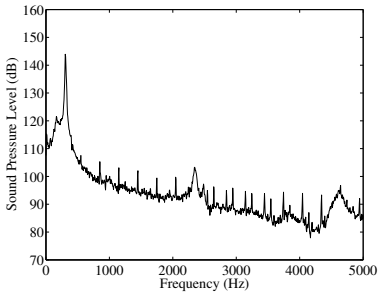

Figure 7. Pressure spectra in the combustion chamber for the OP_{20} case.

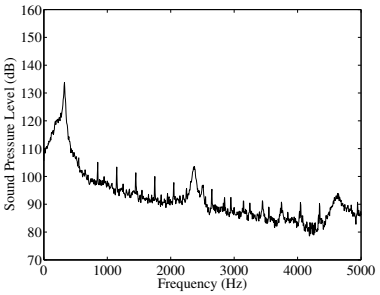

Figure 8. Pressure spectra in the combustion chamber for the $OP_{60}H$ case.

In order to explain quantitatively those differences, detailed planar measurements are performed and the main findings are addressed in the next section.

Planar measurements

In order to understand the underlying flame structure, combined Mie scattering and PIV measurements are performed at a high repetition rate. In parallel and to obtain the position of the flame front, OH-PLIF is performed at a much lower frequency (10 Hz). Those tow approaches may be combined together by a phase-lock approach based on pressure measurements. First, averaged quantities are discussed. In Figure 9 and Figure 10, the mean OH signal is shown in red colors. The mean Mie scattering field is displayed by contours with color changing as function of the magnitude of the axial velocity.

When looking at the results obtained for the OP_{60} case, one can see that the flame front lies in the inner part and that droplets stay on the outer part. The OH signal can be found at the exit of the injection system, indicating that the flame anchoring position is most likely inside the injection system. However, a thermocouple placed on the swirlers does not indicate a specific overheat and therefore it can be concluded that the flame is not attached on the pilot itself. The angle of the flame is around 45 degrees. In non-reacting conditions, the spray had a lower angle. This change in the angular shape of the spray is due to the reactions taking place inside the injection system. A detailed analysis of the He-Ne laser through 1D wavelet decomposition ([9]) shows that the frequency associated to the PVC is very stable around 2580 Hz with fluctuations of the order of 15 Hz. The flame front is not recorded at a distance higher than 50 mm from the exit of the combustor. Another interesting feature is the broadening of the flame front thickness for a distance of 20 mm. This secondary zone corresponds most probably to the reaction of the droplets generated by the multipoint injection system. When performing OH-PLIF for lower staging values (typically 20%), the flame front was only detected for a distance of 20 mm and at a radial position of 20 mm.

Results obtained for $OP_{60}H$ show a completely different behavior (see Figure 10). The flame front is not observed for distances lower than 20 mm from the exit of the injection device. Those results clearly reveal that the flame is lifted in the $OP_{60}H$ case. The region for which OH signal is measured is limited in space. For $OP_{60}H$, it lies within 20 mm whereas it was spreading from about 60 mm for the OP_{60} case. Looking at spray positions, it can be seen that it stays in the inner part while reactions are observed in the outer part of the main flow. The angle of the spray is almost null but with a wider radial spread of the droplets.

Finally, to address the mechanisms of stabilization of the two flames, a detailed analysis of cross-planes are done. As time series data are available, a Dynamic Mode Decomposition ([10]) technique is used to quantify the relative power contained in the PVC as function of distance from the injection system and flame position. In the present case, the QR version of the algorithm is applied to instantaneous Mie scattering images. An overall number of 4313 samples are analyzed. A systematic application of this algorithm showed that the best signal to noise ratio was obtained for a Mie scattering image that was reduced to one fifth in both dimensions as compared to the original one. This results in a spatial resolution of about 2 pixels per mm. No overlap was computed to obtain the new images and the averaged Mie image is not subtracted prior to the DMD analysis. A typical DMD spectra is presented in Figure 11. This spectra is obtained for the non reacting case at a distance of 5 mm from the exit of the injection device. One can readily notice the peak associated to the PVC frequency. The magnitudes of the Koopman modes have been normalized to one with respect to the highest mode for strictly positive frequencies. The signal to noise ratio is defined as being the ratio of the magnitude of the Koopman mode associated to the frequency of interest (here the PVC) with respect to the baseline level, which is measured as being the median of the Koopman modes of the frequencies within 200 Hz of the peak. In the example shown in Figure 11, this leads to a signal to noise ratio around 5.

This analysis is performed for all the planes available and for three different conditions. The first one is the non-reacting (labelled NR in Figure 12). One can see that the signal to noise ratio drops from 5 at 5 mm from the exit to about 1 at 30 mm. Its value is only of 2 for a distance of 20 mm. Most interestingly, the signal to noise ratio associated to the OP_{60} case is much higher than the non-reacting case. Its initial value is of the order of 7 for a distance of 5 mm and drops to about 3 for a distance of 20 mm. It is not detected any further as the signal of Mie scattering is vanishing due to combustion. This result shows that not only the PVC is still present in reacting cases, but that its strength is increased for the OP_{60} case. Results obtained for $OP_{60}H$ show a similar trend with respect to the spatial evolution. The signal is not detected for distances higher than 20 mm. However, it is quite clear that even at the exit of the injection device, the strength of the PVC for $OP_{60}H$ is reduced as compared to non-reacting case. The PVC has a strong role for stabilizing the flame in the case of OP_{60} and this strength is also increased as it is very stable in frequency (see [9]). The PVC will offer a stabilization point for the flame. Due to its precessing movement, this point will slightly move in space (within 1 mm as measured by Mie scattering images). Bigger droplets will be ejected towards the recirculation zone (either inner or outer). This will induce different

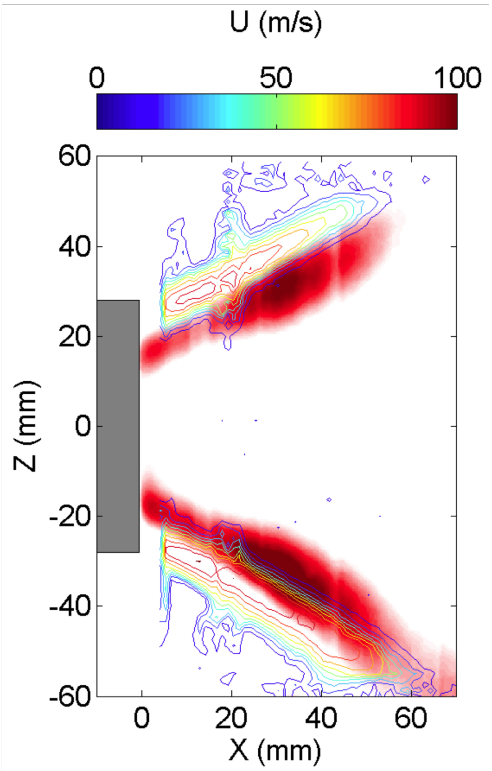

Figure 9. Combined velocity and flame front position for the OP_{60} case.

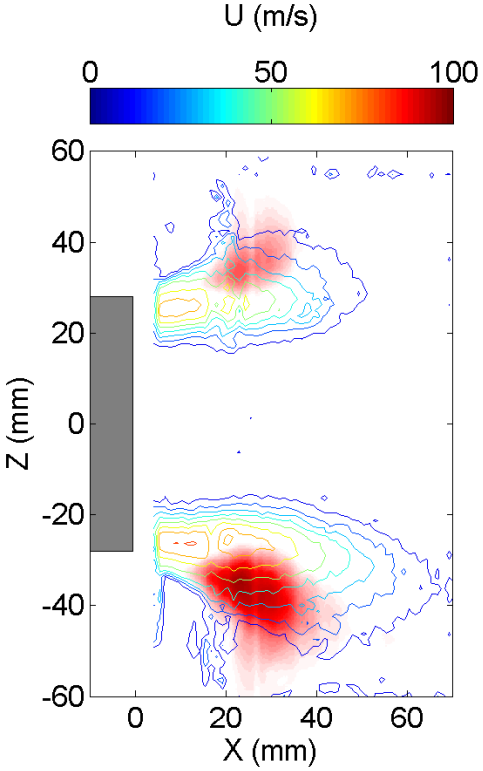

Figure 10. Combined velocity and flame front position for the $OP_{60}H$ case.

radial locations for the main reaction to take place. Those different radial locations will then not be resonant with a quarter wavelength mode and the coupling between the heat release and the acoustic will be reduced. On the opposite, if the PVC is not very strong, the amount of heat release that will be influenced by the precessing movement will be smaller. The main reaction will then take place further downstream, far away from the PVC and may be resonant with the quarter wavelength mode of the combustor. This is the reason for which the $OP_{60}H$ is showing a strong thermo-acoustic oscillation while the OP_{60} has lower amplitudes for the quarter wavelength mode.

Summary and Conclusions

A laboratory-scale staged multi-injection combustor is described in the present paper. Using a staging procedure between the primary pilot stage and the secondary multipoint one, droplet and velocity field distributions can be varied in the spray that is formed at the entrance of the combustion chamber, influencing the dynamics of the flame. The flame stabilization process does not only depend on injection parameters but also on the previous conditions, showing a hysteresis phenomena. Two operating conditions (using identical injection properties) are analyzed. The flame structure and the spray's behavior are characterized using High Speed Particle Image Velocimetry and Planar Laser Induced Fluorescence in the axial and transverse directions. Results show that the flame can be stabilized either in the pilot region or the combustion chamber, leading to a more or less strong thermo-acoustic activity. Both cases reveal the presence of a PVC in the flow that is strongly affected by the acoustic perturbation. Indeed, for the OP_{60} case where the acoustic amplitude is lower, results indicate a behavior of droplet's and flame mainly driven by a strong PVC. However, for the $OP_{60}H$ case, high acoustic perturbations occur leading to a very fluctuating PVC and the flow is mainly driven by the acoustic motion. In the first case, it was shown that PVC is strengthened due to combustion whereas in the second case, it tends to be weakened.

Acknowledgements

This work is supported by Pôle ASTECH and funded by Conseil Régional d'Ile-de-France, in the framework of the INCA (Initiative en Combustion Avancée) initiative. The authors would like to thank the technical staff at the EM2C laboratory for their help in designing and mounting the experimental setup.

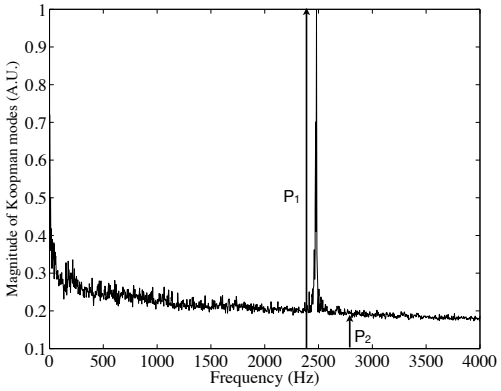

Figure 11. Typical spectra obtained for Dynamic Mode Decomposition based on Mie scattering for the non-reacting case.

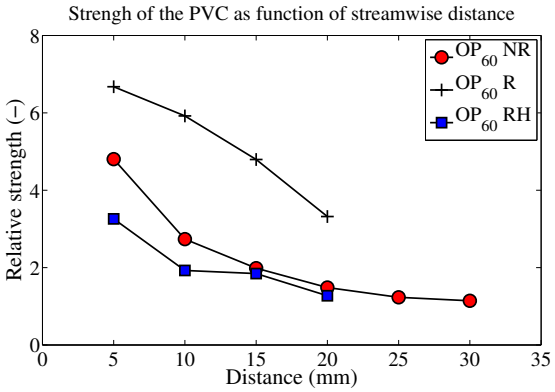

Figure 12. Relative strength of the PVC as function of axial distances for the non reacting, the OP_{60} and $OP_{60}H$ cases.

References

[1] Barbosa, S., Scouflaire, P. and Ducruix, S., *Proceedings of the Combustion Institute* 32:2965-2972 (2009)
[2] Meier, W., Boxx, I., Stohr, M. and Carter, C., *Experiments in Fluids* 49:865-882 (2010)
[3] Shimura, M., Ueda, T., Choi, G-.M., Tanahashi, M. and Miyauchi, T., *Proceedings of the Combustion Institute* 33:775-782 (2011)
[4] de la Cruz Garcia, M., Mastorakos, E., and Dowling, A. P., *Combustion and Flame*, 156:374-384 (2009)
[5] Galley, D., Ducruix, S., Lacas, F., and Veynante, D., *Combustion and Flame* 158:155-171 (2011)
[6] Providakis, T., Zimmer, L., Scouflaire, P., and Ducruix, S., *ASME Turbo Expo 2011: Power for Land, Sea and Air* Vancouver, Canada, June 6-10, 2011
[7] Zimmer, L., Domann, R., Hardalupas, Y. and Ikeda, Y., *AIAA Journal* 41:2170-2178 (2003)
[8] Providakis, T., Bossard, PE, Scouflaire, P., Ducruix, S. and Zimmer, L. (2012) Experimental study of aerodynamic structures in a non-reactive dodecane-air combustor using time resolved PIV, 16th Int Symp on Applications of Laser Techniques to Fluid Mechanics, Lisbon, Portugal, 09-12 July, 2012
[9] Providakis, T., Zimmer, L., Scouflaire, P., Ducruix, S. (2011) Characterization of the coherent structures in swirling flames stabilized in a two-staged multi-injection burner: influence of the staging factor, 3rd INCA colloquim, November 17-18, Toulouse, France
[10] Schmid, P., *Journal of Fluid Mechanics* 656:5-28 (2010)